

View Article Online **PAPER**



Cite this: Soft Matter, 2024, 20, 7471

Received 24th June 2024, Accepted 28th August 2024

DOI: 10.1039/d4sm00772g

rsc.li/soft-matter-journal

Bulking up: the impact of polymer sterics on emulsion stability†

Ashley N. Mapile p and Lawrence F. Scatena ** *

Encapsulation of hydrophobic active ingredients is critical for targeted drug delivery as water-insoluble drugs dominate the pharmaceutical marketplace. We previously demonstrated hexadecane-in-water emulsions stabilized with a pH-tunable polymer, poly(acrylic acid) (PAA), via a steric layer preventing particle aggregation. Using vibrational sum frequency scattering spectroscopy (VSFSS), here we probe the influence of steric hindrance on emulsion colloidal stability by tailoring the molecular weight of PAA and by adding an additional methyl group to the polymer backbone via poly(methacrylic acid) (PMAA) at pH 2, 4, and 6. At low polymer molecular weight (2 and 10 kDa), PAA adsorption is entropy driven and akin to surfactant-mediated stabilization. With 450 kDa PAA, the longer polymer chain emphasizes enthalpically favored polymer-oil interactions to initially coat the surface, and forms layers at increasing molecular weight (1000 and 4000 kDa). PMAA exhibits better oil-solubility than PAA at low concentrations but cannot accommodate the steric hindrance at higher concentrations leading to disorder. Finally, we connect our molecular-level understanding of PAA ordering with temperaturedependent dynamic light scattering experiments and observe that emulsions coated with PAA at pH 2 and 4 maintain colloidal stability from 0-90 °C, making PAA a promising polymer for hydrophobic drug delivery.

Introduction

The inherent hydrophobicity of pharmaceutical ingredients remains a challenge in delivering drugs through the aqueousrich human body. It was estimated in 2007 that 40% of drugs on the market were water-insoluble, with a surge of hydrophobic drug candidates in the development pipeline ($\sim 90\%$) expected to increase the prevalence of oil-soluble pharmaceuticals in the current age. In addition to transporting inherently hydrophobic drugs, using oil-soluble delivery agents protects sensitive ingredients. The recent employment of lipid nanoparticles for delivering the COVID-19 vaccine, for example, protected the mRNA nucleotides from metabolic enzymes and other harsh environments in the body.2 Current mechanisms for hydrophobic drug delivery include inorganic-based nanocarriers,^{3,4} lipid-based nanoparticles,⁵ nanoemulsions coated with surfactants or gelling polymers, 6-8 and protein coronas. 9 While these systems efficiently encapsulate hydrophobic drugs, the mechanism of stabilization is largely unknown. In one respect, these systems defy common theories of colloidal stability (i.e. DLVO) that require a substantial surface charge to prevent particle aggregation.

University of Oregon Department of Chemistry and Biochemistry, 1253 University of Oregon, Eugene, OR 97403, USA. E-mail: scat@uoregon.edu † Electronic supplementary information (ESI) available. See DOI: https://doi.org/ 10.1039/d4sm007729

Additionally, in the case of proteins or diverse lipid bilayers, specific probing of the moieties that give rise to colloidal stability is difficult due to the chemical complexity of the stabilizing units and the buried nature of droplet interfaces. We recently demonstrated that small emulsion droplets suspended in water exhibit long-term colloidal stability when coated with poly(acrylic acid) (PAA) at pH 2 and 4.10 With surface-specific spectroscopy, it was determined that low-charge PAA stabilizes emulsions through an ordered backbone that provides steric repulsion between droplets. These emulsions are resistant to acidic conditions and the addition of electrolyte. Using a simple polymer like PAA allows for a detailed experimental view of molecular ordering at the droplet interface with insight that can be applied to more complicated polymers or proteins that contain many different chemical functionalities.

Due to their tunable molecular weight, pH sensitivity, and unique architectures of synthetic polymers, 11 kinetically stable droplets coated with polymer are becoming increasingly useful for biosensing applications. 12 While changing the macromolecular concentration can impact emulsion stability, 13 many polymers exhibit poor solubility at higher concentrations. Instead, probing different chemical architectures or conformational orientation at an interface is achieved through polymer morphology (i.e. linear, 14 block, 15,16 or core-shell 17), chemical identity/compatibility, 18,19 and layer thickness. 20-22 In particular, the thickness of a polymer layer at an interface is adjusted by modifying the polymer molecular weight or by adding

Paper Soft Matter

chemical moieties to the polymer backbone, both of which increase steric hindrance and have the ability to stabilize emulsions. Understanding how polymers with varying steric properties orient at an interface will provide insight into structure-function relationships for drug delivery platforms, especially with polymers that have pH tunability relevant to physiological conditions.

The adsorption behavior of polymers has generated both theoretical²³ and experimental^{24,25} studies that seek to understand interfacial conformation. In particular, a "train, loop, tail" representation has been developed that describes how polymers lie flat at the surface (train), coil beyond the surface into the bulk (loop) and extend at the ends of the polymer chains (tail) to emphasize favorable surface-polymer interactions or bulk-polymer interactions, dependent on the polymer identity and interface.²⁶⁻²⁸ To probe polymer conformation at interfaces, vibrational sum frequency spectroscopy (VSFS), a surface-specific vibrational spectroscopy that provides insight to molecular ordering at buried interfaces, has been employed. Previous sum frequency studies have investigated the influence of polymer molecular weight on backbone ordering at the planar polystyrene/silver interface, 29 air/water interface, 30 and oil/water interface.31 These studies found that polymer ordering was highly dependent on a balance between enthalpic and entropic contributions to polymer adsorption. For ionic polymers, solvation in the bulk phase is favored over adsorption to the interface. In solution, entropic disorder of the polymer chain can be leveraged and the charged functional groups can be better solvated without the steric hindrance exhibited at the interface. Thus, enthalpically induced adsorption and solvation of the side chain functional groups must overcome this barrier to drive polymer adsorption to surfaces.³² Specifically, enthalpic contributions from backbone/substrate interactions would increase interfacial ordering while entropic contributions from polymer coiling would reduce interfacial ordering.²⁹ While delivering a useful mechanistic groundwork for understanding polymer adsorption, a key limitation of the previous sum frequency studies is that only 2-3 different molecular weights were studied thus, limiting the extent of steric hindrance applied to the system. Further, studies at the planar interface neglect the role of particle stabilization and view macromolecules as thermodynamically adsorbed. In droplet systems however, ultrasonication imparts energy to accelerate the diffusion of polymers to the surface and subsequently, the colloidal system is governed by DLVO theory which can influence polymer conformation. These factors highlight the necessity to understand molecular ordering and nuances of the droplet interface that are not included in the planar sum frequency geometry.

In addition to tuning molecular weight, polymer steric hindrance can be increased with the addition of bulky groups to the polymer backbone. The few studies that have investigated the interfacial ordering of a sterically hindered polymer backbone through methyl substitution (i.e. poly(acrylic acid) vs. poly(methacrylic acid) or poly(methyl methacrylate)) have only been conducted via bulk infrared spectroscopy³³ or at planar air/water^{34,35} or oil/water interfaces^{36,37} with VSFS. These studies found that the addition of a methyl group on the polymer backbone improves solvation of the polymer into the hydrophobic phase. Additionally, changing the stereo configuration of the polymer, through the use of isotactic and syndiotactic poly(methacrylic acid), for example, can result in distinct oiland water-rich C=O environments. For simplicity, this work uses isotactic poly(methacrylic acid), but future work will seek to understand the influence of backbone substitution orientation on polymer conformation at curved interfaces.

In this work, poly(acrylic acid) of five different molecular weights (2, 10, 450, 1000, and 4000 kDa) was used to probe the influence of steric hindrance on polymer molecular ordering at a droplet interface. The hexadecane/water emulsion interface used in this work mimics drug delivery platforms where a hydrophobic drug is incapsulated in the oil-core. Vibrational sum frequency scattering spectroscopy (VSFSS) is used to provide molecular-level detail of ordered vibrational modes at the curved interface while complementary dynamic light scattering (DLS) provides insight to emulsion stability. Additionally, we investigated the role of an extra methyl group on polymer ordering by measuring emulsions coated with poly(methacrylic acid) at varying concentrations. Based on rheological and thermal testing of bulk polymers, 38-41 it is hypothesized that at the oil/water droplet interface polymers of a low molecular weight will exhibit surface activity similar to that of surfactants and exhibit minimal polymer-polymer interactions. At higher molecular weights, it is projected that the polymer will have interchain crosslinks that contribute to layering on the droplet. At any molecular weight, the balance between enthalpically favorable polymer-substrate or polymer-polymer interactions and entropically favorable polymer disorder in the aqueous phase will determine the interfacial conformation of the polymer and the resulting emulsion stability. Finally, pH- and temperaturedependent DLS measurements of emulsion stability connects the microscopic understanding of polymer steric hindrance on interfacial ordering to macroscopic insight leading to the development of stable drug delivery systems.

Materials and methods

Materials

All materials were used as delivered without further purification. Hexadecane (\geq 99%), dioctyl sodium sulfosuccinate (AOT, \geq 97%), and poly(acrylic acid) (PAA, average $M_{\rm v} \sim 450$ kDa) were purchased from Sigma-Aldrich. PAA of varying molecular weight (ultra pure 2 kDa, ultra pure 10 kDa, 1000 kDa, and 4000 kDa) and poly(methacrylic acid) (PMAA, 100 kDa) were purchased from Polysciences, Inc. Deuterated hexadecane (n-hexadecane- d_{34} , 98.6% D), sodium deuteroxide (NaOD, 99.5% D), and deuterium chloride (DCl, 99.8% D) were purchased from CDN Isotopes. Deuterium oxide (D₂O, 99.9% D) was purchased from Cambridge Isotope Labs. All glassware was cleaned with a sulfuric acid bath (98%, Sigma-Aldrich) containing ALNOCHROMIX oxidizer from Godax Laboratories Inc.

Glassware was submerged in the acid bath for at least 24 hours before being rinsed with 18.2 MΩ-cm water and dried in an oven.

Emulsion formation

Hexadecane (or D-hexadecane) emulsions suspended in water (or D2O) were prepared by ultrasonication from a Branson Sonifer 250 at 5% output power of 20 kHz for 5 minutes at a constant duty cycle. The ultrasonicating probe tip was aligned at the interface of the aqueous solution and oil layer to ensure homogenous mixing. The AOT-coated emulsion standard was formed by ultrasonicating an AOT stock solution with D-hexadecane to generate an emulsion with 1 mM AOT and 2.5% v/v oil in water. Polymer-coated emulsions were formed in the same fashion with DCl or NaOD added to reach the desired pD (pH). Emulsion pH was measured using Millipore Sigma MColorpHast pH strips. While the detection of pH values can differ from pD values by 0.43,42 pH instead of pD is used for clarity and accurately describes the pH-dependent phenomenon at three regions studied as confirmed by previous work from this group.

Dynamic light scattering and zeta potential

Hydrodynamic diameter (Z-average), polydispersity index (PDI), and zeta potential of the emulsions was measured with a Malvern Zetasizer Nano ZS. The size and PDI are reported from an average of at least three measurements while zeta potential values are an average of at least five measurements. Room temperature DLS and zeta potential measurements were collected by pipetting 1 mL of the emulsion solution into a Malvern folded capillary zeta cell without dilution. For variable temperature DLS, 1 mL of emulsion solution was pipetted into a glass cuvette and capped. The samples are prepared at room temperature and equilibrated for at least 20 minutes before the first measurement occurs at 0 °C. DLS measurements are taken at 10 °C increments (up to 90 °C) with sufficient equilibration time at each temperature step to ensure temperature accuracy with 0.1 $^{\circ}$ C.

Vibrational sum frequency scattering spectroscopy

The second-order non-linear spectroscopy technique, vibrational sum frequency scattering spectroscopy (VSFSS) provides molecular-level information on the population and ordering at curved interfaces. 43,44 A sum frequency response is only generated in non-centrosymmetric environments, such as an interface, and is forbidden in bulk media. 45,46 The VSFSS experimental setup used here has been describe thoroughly in recent publications from the Richmond/Scatena and Brozek laboratories. 10,47 A schematic of the laser experiment is provided in Fig. S1 (ESI†). Briefly, an 800 nm, ~80 fs fundamental pulse with a 1 kHZ repetition rate is generated from a Ti:Sapphire regenerative amplifier laser system (Coherent Libra). This fundamental beam is split with a portion being used as the visible pulse and the remaining sent through an optical parametric amplifier (Coherent OPeRA Solo) to generate broadband IR pulses via difference frequency generation. The IR pulse is

focused to the sample at a spot size of $\sim 80 \mu m$ while the visible is focused after the sample cell to a $\sim 500~\mu m$ spot size. The sample cell consists of a CaF₂ window (front) and quartz cuvette (back, Helma QS), with an optical path length of 200 μm. The scattered sum frequency response is collected at $\sim 60^{\circ}$, collimated with a plano-convex lens, and focused into a spectrograph and CDD intensifier (Princeton Instruments IsoPlane SCT320 and PI-MAX4). Visible pulse energy is 25 µJ while IR pulse energies are 5 μJ and 2-3 μJ for the C-H and C=O stretching regions, respectively. All spectra were collected in the ssp polarization combination (corresponding to the polarization of the sum frequency, visible, and IR pulses, respectively), consistent with previous sum frequency experiments measuring polymer molecular ordering. 10,48-50 For our experiments, the ssp polarization scheme provides us with substantial information on molecular ordering without complicating the spectral response.

A single VSFS trace is an average of at least 3 trials measured on different days. One experimental trace consists of 2 signal and 2 background measurements of 20 minutes each that accounts for daily fluctuations in laser power. Each trial is averaged, background subtracted, and normalized by a nonresonant response from KNbO3 nanoparticles. In the C-H region, spectra are normalized by the integrated intensity from 2800–3000 cm⁻¹ generated from a reference D-hexadecane emulsion in D₂O with 1 mM AOT. Each trial is additionally normalized by the size of the emulsion (determined by a monomodal DLS distribution) through a scattering pattern developed by Roke et al. which accounts for the percentage of scattered light collected at 60°. 51,52 Collection of the scattered sum frequency at 60° also induces incomplete phase matching in the far field at the detector. 43,53 The coherence length of the experiment is much longer than that of the droplet radius allowing for deconstructive interference from molecular dipoles across the droplet to be avoided. Additional details on the normalization procedure is in previous publications from the Richmond/Scatena group. 54,55

The intensity of the scattered vibrational sum frequency response is proportional to the intensities of the incoming visible and IR beams $(I_{IR}I_{vis})$ and the square modulus of the second-order nonlinear susceptibility $(X^{(2)})$. Bain et al. developed a rigorous equation accounting for the non-resonant and resonant contributions of $X^{(2)}$ (eqn (1)) and is used for fitting the VSFSS spectra here.56

$$\left| X(\omega)^{(2)} \right|^2 = \left| X_{NR}^{(2)} e^{i\phi} + \sum_{\nu} \int_{-\infty}^{+\infty} \frac{A_{\nu} e^{i\phi \nu} e^{-\left(\frac{\omega_L - \omega_{\nu}}{\Gamma_{\nu}}\right)^2}}{\omega_L - \omega_{IR} + i\Gamma_L} d\omega_L \right|^2 \tag{1}$$

In eqn (1), the amplitude of the non-resonant susceptibility $(X_{NR}^{(2)})$ has a phase ϕ . The resonant susceptibility is described by the summation of all sum frequency active vibrational transitions, A_{ν} is the peak amplitude, ϕ is the phase, Γ_L is the Lorentzian linewidth describing homogenous broadening, and Γ_{ν} is the Gaussian linewidth describing inhomogeneous **Paper**

broadening. Tables S3-S6 (ESI†) describe the fitting parameters used in this paper.

Results and discussion

Emulsions coated with PAA of varying molecular weight

Emulsion characteristics. A solution of poly(acrylic acid) (PAA) in D₂O at varying molecular weight (2, 10, 450, 1000, and 4000 kDa) was ultrasonicated with 2.5% p-hexadecane to form kinetically stable emulsions with a final polymer concentration of 500 ppm. Our previous study investigated the influence of concentration on emulsion stabilization. 10 Briefly, 500 ppm was chosen as enough polymer concentration to coat the interface but reduce the amount of polymer layering that causes charge screening. We seek to limit charge screening so that approximately a single layer of polymer is adsorbed to the interface. This allows for zeta potential to be used as a metric for understanding polymer adsorption. The size, polydispersity index (PDI), and zeta potential of the resulting emulsions prepared at pH 2, 4, and 6 are summarized in Fig. 1. Bare emulsions, oil droplets without a surfactant or polymer coating, are very unstable and result in hydrodynamic diameters near 1000 nm. With the addition of stabilizing surface-active agents, such as surfactant or polymer layer, emulsion sizes converge between 200-500 nm and exhibit long-term colloidal stability. 10,57 With this criteria in mind, stable emulsions were formed at pH 4 with all molecular weights and at pH 2 for low molecular weights (≤450 kDa) as indicated by the small size (Fig. 1A) and visual turbidity. At pH 2, large unstable oil droplets were formed with high molecular weights (1000 and 4000 kDa) as indicated by the large sizes. No stable emulsions were formed at pH 6. Similarly, emulsions formed at pH 4 and 2 exhibit moderate polydispersity with a PDI around 0.4 (Fig. 1B) while pH 6 emulsions are very polydisperse. The most monodisperse emulsions were formed with the shortest chain polymer, 2 kDa, due to the reduced crosslinking and layering exhibited by the higher molecular weight polymers.

At pH 4 and 6, an absolute minimum of the zeta potential was observed at 450 kDa (Fig. 1C). With shortening or lengthening of the polymer chain the zeta potential is decreased in magnitude. At lower molecular weights, the decline in surface charge is attributed to the reduced polymer surface coverage given the same concentration as higher molecular weights counterparts.⁵⁸ At higher molecular weights, charge screening of multiple polymer layers causes a reduction in zeta potential. At pH 2, very little change in zeta potential was observed due to the low percent deprotonation in these conditions (1%). The hydrodynamic diameter and zeta potential are important parameters for contextualizing our spectral results below, while size distribution was used to account for the scattered signal collected by VSFSS.

Entropy and enthalpy favored adsorption. To understand the changes in PAA conformation as a function of molecular weight, we turned to well-known mechanisms of polymer adsorption to analyze the VSFS spectral trends below. Unlike

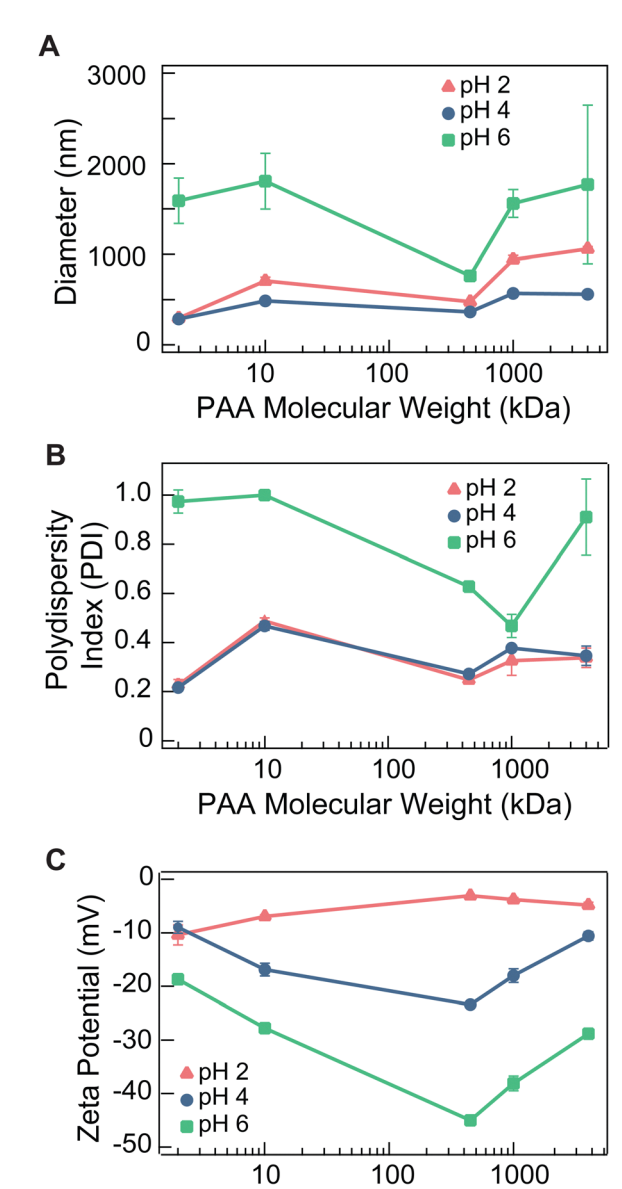


Fig. 1 (A) Hydrodynamic diameter, (B) polydispersity index, and (C) zeta potential of emulsions coated with 500 ppm poly(acrylic acid) at varying molecular weights and pH conditions.

PAA Molecular Weight (kDa)

surfactants, polymers are not inherently surface active as they do not always possess distinct hydrophilic and hydrophobic regions as these regions are continuously tethered. Recent work has suggested that polymer adsorption is driven by reducing the unfavorable hydrophobic-water contacts at the interface.⁵⁹ In other words, the polymer helps to solubilize the high-energy oil droplet, shields these solvent-substrate interactions, and reduces the interfacial tension. While our pendant drop surface tensiometery (Fig. S4, ESI†) cannot serve as a direct representation of polymer adsorption at the emulsion interface due to the kinetically stable droplet formed by ultrasonication, this shielding mechanism is likely promoting polymer adsorption. We contextualize the adsorption phenomenon further by considering the enthalpic and entropic gains from polymer adsorption.

Soft Matter Paper

In a similar fashion to denatured proteins, polymers would rather be solvated in the bulk, aqueous phase to emphasize entropic disorder, solvate ionic functional groups, and screen hydrophobic moieties. Therefore, to promote polymer adsorption to surfaces, the strong polymer-water interaction must be overcome by favorable polymer-substrate or polymer-polymer (layering) connections, which are closely tied to polymer length. Previous work has demonstrated that at high molecular weights, long polymer chains can extend at surfaces. This extension emphasizes favorable polymer-polymer and polymer-substrate van der Waals forces which results in an ordered backbone.²⁹ On the other hand, at low molecular weight, the conformation of the adsorbed polymer favors entropic disorder. With less repeat units, there are fewer backbone/substrate interactions as compared to higher molecular weight systems, thus entropy must compensate. These behaviors are described as entropy and enthalpy-driven adsorption, identifying the driving force that dictates polymer conformation at the interface.

The mechanism for adsorption is described quantitatively by the unit-less critical adsorption parameter, δ_c , and was calculated for the PAA system studied here (Fig. 2) where $\delta_{\rm c} \sim N^{-3/5}$ and N is the degree of polymerization.²⁹ A larger δ_c suggests more entropic contributions to adsorption while a lower δ_c indicates more enthalpic contributions. We find that PAA adsorption is entropically driven at low molecular weights (2 and 10 kDa) and enthalpically driven at high molecular weights (450, 1000, and 4000 kDa). This analysis suggests that at low molecular weight, a preference towards disorder is expected and at higher molecular weights, an extended ordered backbone is favored.

VSFSS of varying molecular weight PAA emulsions at pH 4. A conformational analysis of PAA at the oil/water droplet interface as a function of molecular weight was probed with vibrational sum frequency scattering spectroscopy (VSFSS). This technique provides a molecular picture of droplet interfaces

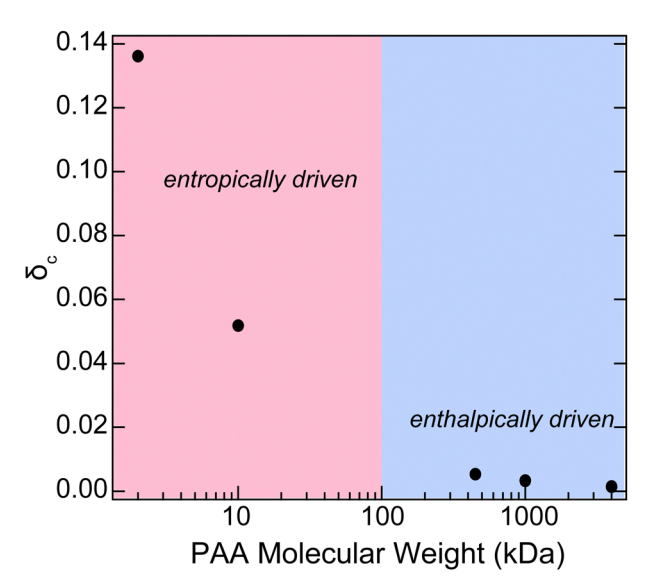


Fig. 2 Critical adsorption parameter ($\delta_{\rm c}$) as a function of poly(acrylic acid) molecular weight. $\delta_{\rm c} \sim N^{-3/5}$ where N is the degree of polymerization.

by probing interfacial vibrations, where the presence of sum frequency signal indicates population and net orientation of the vibrational transition moments being probed. The polarization scheme ssp (relating to the polarization of the sum frequency, visible, IR pulses, respectively) was used to probe vibrational transition moments perpendicular to the oil/water interface, as consistent with previous experiments. 10 Fig. 3 and 5 show the interfacial vibrational response of the PAA backbone in the C-H stretching region as a function of molecular weight at pH 4 and pH 2, respectively. As stable emulsions were not formed in pH 6 conditions, no VSFSS measurements were conducted.

At pH 2 and 4, a narrow feature at 2932 cm⁻¹ is attributed to the methylene (CH₂) symmetric stretch on the backbone of PAA while the broad feature at 2871 cm⁻¹ is assigned to the methine (CH) stretch. These fitting assignments are consistent with previous literature and fitting parameters are summarized in Table S2 (ESI†). 10,50 To deconvolute the influence of polymer molecular weight on interfacial ordering, the peak amplitude and Gaussian linewidth were compared as a function of molecular weight (Fig. 3B and C). As the oscillator probed in these experiments is kept consistent for each measurement, the peak amplitude provides information on the population and orientation of vibrational modes while the Gaussian linewidth provides insight into the variety of chemical environments present for these vibrations at the droplet interface. For example, a large amplitude suggests a high population of ordered surface vibrational modes and a small Gaussian linewidth suggests a limited chemical environment of those moieties. The higher intensity of the methylene symmetric stretch, as compared to the methine stretch, makes it a better probe for determining interfacial ordering as a function of polymer molecular weight. However, the trends for the methine stretch were included to show that the conclusions generated on polymer ordering is consistent regardless of the vibrational probe chosen for analysis.

In general, the conformation of PAA at pH 4, as compared to pH 2, is driven by the polymer's preference to solvate the ionic species. As detailed below, the conformational changes as a function of molecular weight at pH 4 are much more dramatic than at pH 2. At pH 4, the peak amplitude of the CH₂ symmetric stretch (ss) exhibits a maximum at 450 kDa and decreases with either the lengthening or shortening of the polymer chain (Fig. 3A and B). These results closely resemble the trend exhibited with zeta potential as a function of molecular weight, where high molecular weight polymers layer at the surface and charge screen the slipping plane. The high intensity VSFS signal for the CH₂ ss at 450 kDa suggests a very ordered polymer backbone, consistent with previous interfacial studies. 10 When increasing the polymer molecular weight, the peak amplitude decreases due to disordered interchain crosslinking. While some layering can be ordered, the necessity to accommodate deprotonated acid groups results in more incomplete and random polymer sheets, which is not seen at pH 2. This PAA layering is supported by the increase in hydrodynamic size measured by DLS (Fig. 1A). Interchain interactions are

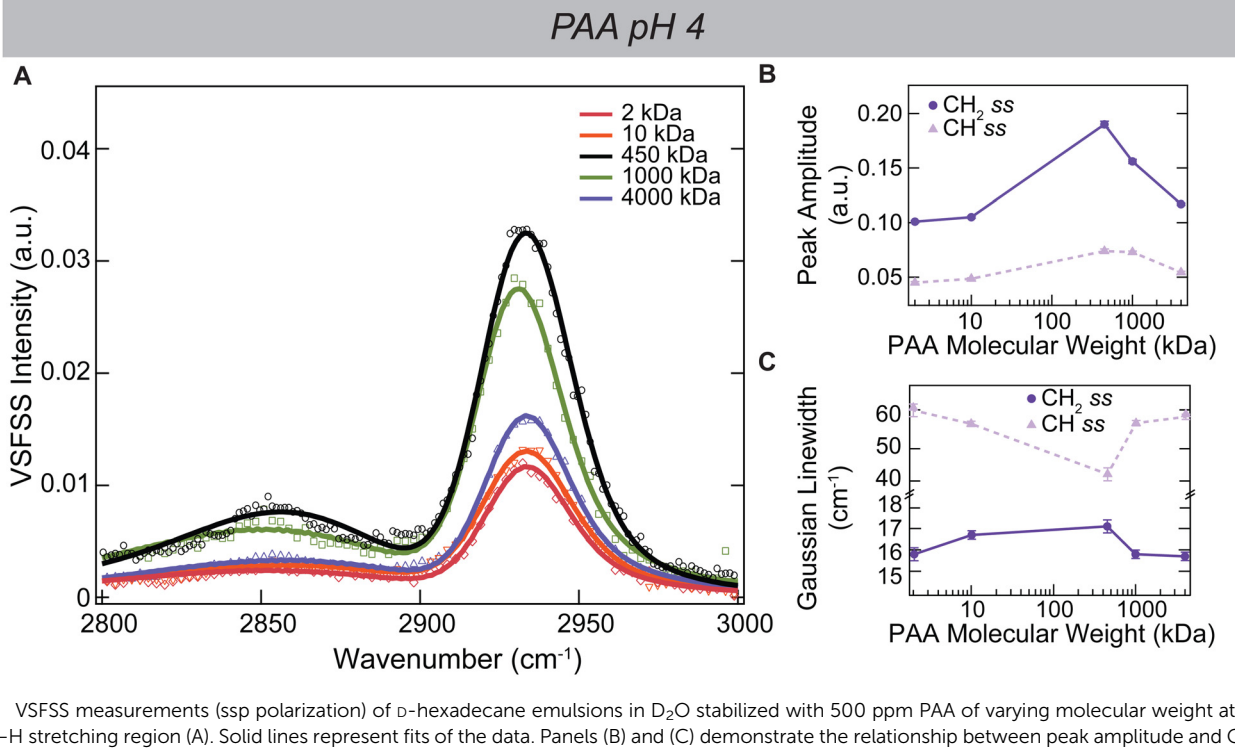


Fig. 3 VSFSS measurements (ssp polarization) of D-hexadecane emulsions in D₂O stabilized with 500 ppm PAA of varying molecular weight at pH 4 in the C-H stretching region (A). Solid lines represent fits of the data. Panels (B) and (C) demonstrate the relationship between peak amplitude and Gaussian linewidth obtained from the fits as a function of PAA molecular weight for the CH2 and CH symmetric stretch.

frequently exhibited for high molecular weight polymers in bulk solution, where an increase in mechanical robustness and viscosity is attributed to crosslinking. 40,41

At lower molecular weights, the CH₂ peak amplitude decreases due to conformational adjustment of the polymer that is necessary to solvate the deprotonated carboxylic acids on the short chain and is entropy favored. Additionally, it is likely that lower molecular weight PAA is less surface active and thus there is less interfacial population that would give rise to VSFS amplitude.⁵⁸ Previous studies have demonstrated that long-chain polymers emphasize the positive enthalpic interactions between the polymer backbone and the substrate (in this case, hexadecane).31,60 At low molecular weights, this long-range communication is disrupted and thus shorter PAA chains cannot utilize the strong enthalpic interactions leveraged by longer chain polymers. Instead, it is hypothesized that low molecular PAA is coiled at the interface in a disordered orientation that is both entropy favored and solvates the deprotonated acid.

The change in Gaussian linewidth for the CH₂ ss at pH 4 is minimal ($\pm 2 \text{ cm}^{-1}$) as a function of molecular weight (Fig. 3C) due to this vibrational mode being solvated completely in the oil phase and disconnected from the C=O functional group. However, the methine stretch exhibits a unique trend and is inherently broader than the methylene stretch, as this mode is tethered to the water-soluble carboxylic acid group whose solvation environment varies significantly. The increase in Gaussian linewidth for the CH stretch as we move to the lower and higher extremes of molecular weight suggest a wider variety of C=O solvation environments. 10,61 The broadening of the methine mode at higher molecular weights is caused by C=O modes being solvated at varying distances and degrees of hydrophobicity as the long chain polymer layers at the surface. At lower molecular weights, the deprotonated acid pulls the short chain further into the water phase, causing the polymer to be adsorbed to the surface like a surfactant (Fig. 4). The different solvation environments due to this ionic group result in linewidth broadening. A similar behavior was observed for short chain zwitterionic polymers at the planar hexadecane/water interface, where the ionic species were solvated in the water and the polymer chain was suspended in the oil, but the intertwined nature of the polymer resulted in mixed solvation phases.⁶²

In general, for pH 4 at low molecular weights, PAA adsorption mimics that of a surfactant with a distinct hydrophobic and hydrophilic region, whereas at higher molecular weights polymer-polymer layering is induced by interchain crosslinking (Fig. 4). These results are similar to a physiologicallyrelevant study that found that Pickering emulsions coated with the polysaccharide, dextran sulphate, were more stable with a molecular weight of 500 kDa than 40 kDa. 63 Our results expand on the influence of polymer steric bulk by finding that at high molecular weights interchain crosslinks cause polymer layering at the surface.

VSFSS of varying molecular weight PAA emulsions at pH 2. At pH 2 (Fig. 5), the interfacial ordering trend as a function of molecular weight is not as clear as at pH 4. However, these minimal changes are not surprising considering that there is such little surface charge on the PAA-coated emulsion at pH 2 (Fig. 1C). Ultimately, the differences in adsorbed PAA

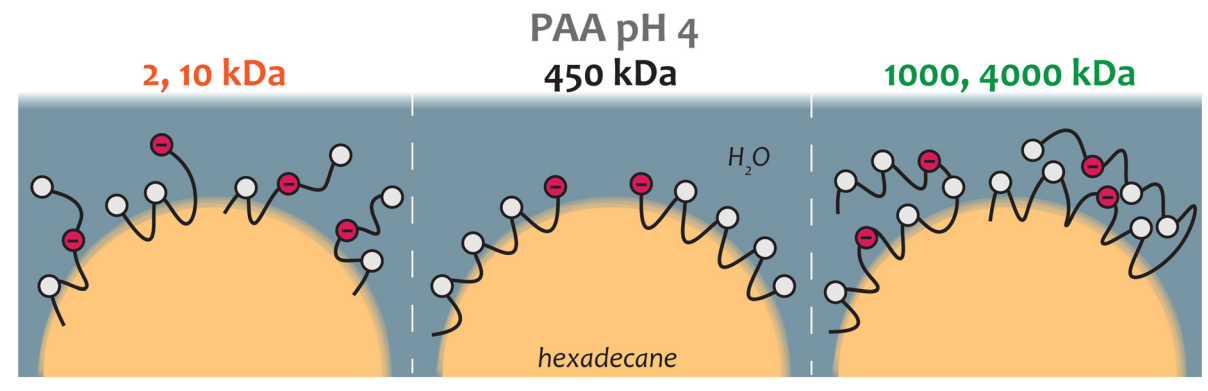


Fig. 4 Molecular picture of the hexadecane/water droplet interface of PAA at low (2 and 10 kDa), medium (450 kDa), and high (1000 and 4000 kDa) molecular weight at pH 4. Red and white circles represent deprotonated and protonated acid groups, respectively.

conformation arising between pH 4 and pH 2 are dictated by the necessity for the pH 4 system to solvate the deprotonated acid. Nearly all of the carboxylic acid is protonated at pH 2 (99%), therefore the conformational adjustments needed to accommodate that charge at pH 4 are not observed. Additionally, there is more surface coverage at pH 2 as compared to pH 4 due to the increase in protonation as confirmed by surface tension measurements (Fig. S4, ESI†) and the higher CH2 ss signal intensity.

At low molecular weight, the entropically-induced adsorption of PAA at pH 2 results in a slight decrease in methylene and methine peak amplitudes as compared to 450 kDa (Fig. 5B). However, this amplitude is still higher than seen at pH 4, as the impacts of entropy are not as dramatic when the polymer is nearly 100% protonated at pH 2. Therefore, despite being entropically driven, the protonation of almost all the acid groups allows PAA to develop a more elongated conformation at pH 2 to better emphasize polymer-substrate interactions as compared to pH 4.

At high molecular weight PAA in pH 2, we attribute the methyl signal intensity to an increase in polymer layers at the emulsion surface. It is known that crosslinking is favorable at pH 2 due to the low percentage of deprotonation, resulting in a high number of polymer-polymer enthalpic interactions. While at pH 4, the addition of polymer layers reduced SFG signal due to disordered packing needed to accommodate the deprotonated acid, PAA at pH 2 can form nearly perfect layers of ordered polymers without ionic functional group disruption. SFG studies of poly(methyl methacrylate) at the planar polymer/ silica surface also find that at high molecular weight, the methylene groups on the backbone are closely packed into the hydrophobic phase and are well oriented.⁶⁴ Additionally, nonionic polymers, like poly(N-vinyl acetamide) are known to exhibit well-ordered layers beyond the droplet surface.²¹ This analysis is supported by the fact that DLS reports large diameters (>900 nm) for droplets formed at pH 2 with high molecular weight PAA. The increase in hydrodynamic diameter is attributed to an increase in polymer layering at the surface, as was seen in previous emulsion studies. 48 At pH 2, the change in CH_2 ss linewidth is minimal (± 2 cm⁻¹) (Fig. 5C), however,

the CH stretch linewidth increases at higher molecular weights. Like in pH 4 conditions, the broadening of this feature is due to the methine mode being tethered to the C=O group. Ultimately, the conformational differences between PAA molecular weights at pH 2 is not as striking as pH 4 due to the polymer being nearly 100% protonated and thus no ionic species require water solvation. A detailed interpretation of the data though, shows that increased surface coverage of PAA is exhibited at lower molecular weights resulting in a fairly ordered backbone, while at higher molecular weights, the increase in spectral intensity is due to polymer layers increasing the ordered population (Fig. 6).

C=O region and summary. To determine the influence of polymer molecular weight on carboxylic acid ordering at the oil/ water emulsion interface, VSFSS was used in the C=O stretching region (Fig. S2, ESI†). As stable emulsions were not formed at pH 6, no VSFSS measurements were conducted. This region requires de-timing of the visible beam to reduce a non-resonant response caused by the windows used in the experiment and detailed in previous publications.54,65 To account for the elevated non-resonant background, two additional broad peaks were used in fitting (Table S3, ESI†). A single resonant feature around 1740 cm⁻¹ is attributed to the C=O stretching mode on PAA. At pH 2 and 4, there seems to be no correlation between the ordering of the C=O mode on PAA and the molecular weight. Global fitting and subsequent analyses of the peak position, Gaussian linewidth, and peak amplitude were all considered (Fig. S3, ESI†). We hypothesize that carboxylic acid ordering is independent of polymer backbone ordering and is nearly undetectable at the oil/water emulsion interface at a concentration of 500 ppm, as shown previously.10 While increasing the concentration of polymer could improve the signal intensity measured by VSFSS, the solubility of high molecular weight PAA decreases dramatically with increasing concentration. Complementary surface-specific techniques, such as vibrational sum frequency spectroscopy at a planar oil/water interface which has increased resolution and input power, could provide better insight into the molecular ordering of the carboxylic acid group on PAA but directly probing this mode on a curved interface at this concentration remains elusive.

Paper Soft Matter

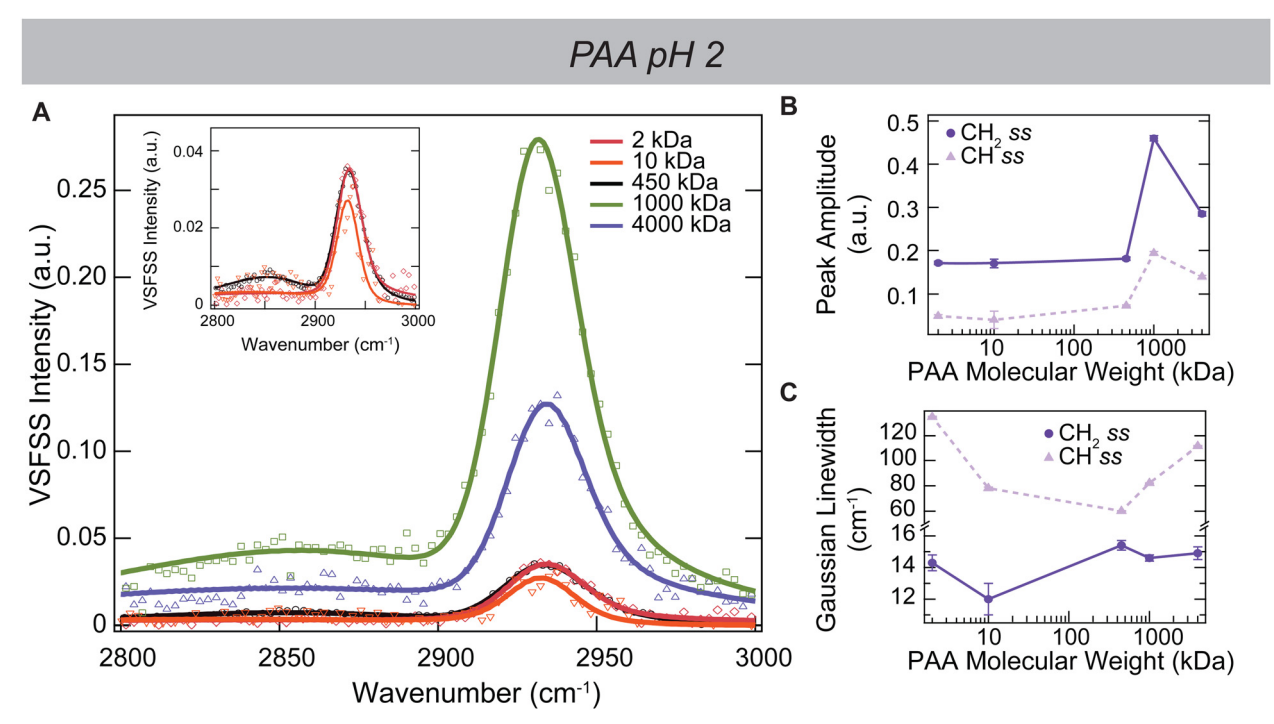


Fig. 5 VSFSS measurements (ssp polarization) of D-hexadecane emulsions in D_2O stabilized with 500 ppm PAA of varying molecular weight at pH 2 in the C-H stretching region (A). Solid lines represent fits of the data. Panel (A) inset provides a zoom-in of the 2, 10, and 450 kDa traces. Panels (B) and (C) demonstrate the relationship between peak amplitude and Gaussian linewidth obtained from the fits as a function of PAA molecular weight for the CH_2 and CH symmetric stretch.

Ultimately these results suggest that at pH 4, PAA exhibits the highest amount of interfacial ordering and subsequent emulsions stability (as indicated by size, PDI, and zeta potential) at 450 kDa. At lower molecular weights, PAA is less-ordered due to poor chain communication resulting in less enthalpically-favored polymer-substrate interactions and greater entropy-favored disorder. At higher molecular weights, PAA becomes less ordered due to enhanced opportunities for crosslinking of polymer chains. Similar behavior is exhibited at pH 2, but with less dramatic interfacial effects as a function of PAA molecular weight due to the lower degree of deprotonation.

It was observed that at low molecular weights, PAA adsorption at pH 2 is well-ordered. At pH 2 with higher molecular weights, the crosslinking-induced environment results in a thick polymer layer at the surface. While not accounted for in the critical adsorption parameter, δ_c , these results suggest that specific chemical nature, tuned by pH in this case, impacts polymer adsorption characteristics.

Emulsions coated with PMAA

Emulsion characteristics. Probing the impact of backbone sterics on interfacial ordering was achieved by ultrasonicating a

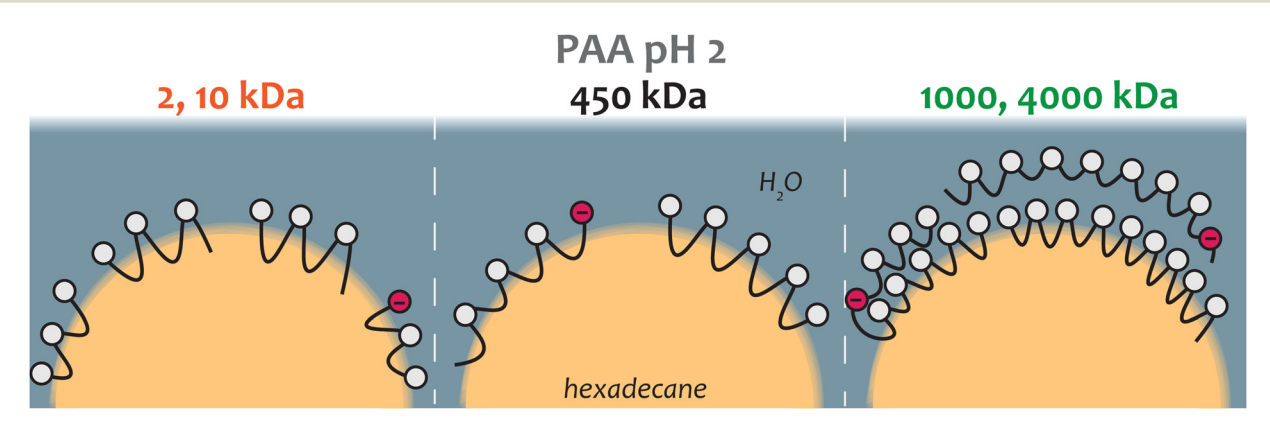


Fig. 6 Molecular picture of the hexadecane/water droplet interface of PAA at low (2 and 10 kDa), medium (450 kDa), and high (1000 and 4000 kDa) molecular weight at pH 2. Red and white circles represent deprotonated and protonated acid groups, respectively.

solution of poly(methacrylic acid) (PMAA, molecular weight = 100 kDa) with D₂O and D-hexadecane to form kinetically stable emulsions with a final PMAA concentration of 500 or 2687 ppm. 500 ppm was chosen to maintain the same concentration as the PAA studies conducted with a molecular weight of 450 kDa, while 2687 ppm was chosen to result in the same number of monomer units of PMAA as compared to PAA at 500 ppm. The surface activity of PAA and PMAA at 500 ppm are similar at pH 2, 4, and 6 (Fig. S4, ESI†) as measured by pendant drop surface tensiometery. Stable emulsions were formed with both 500 and 2687 ppm PMAA at pH 2 and pH 4 (Table S1, ESI†). No stable emulsions were formed at pH 6 regardless of PMAA concentration, however a short-lived emulsion could be formed at pH 6 with 2687 ppm PMAA, likely due to a high surface coverage of the polymer.

VSFSS of PMAA coated emulsions

To determine the influence of steric hindrance on polymer backbone ordering at the oil/water droplet interface, VSFSS was used to measure the interfacial ordering of PMAA as compared to PAA. Fig. 7 shows the interfacial vibrational response of PMAA as a function of pH and concentration in the C-H and C=O stretching regions for both 500 and 2687 ppm. As stable emulsions were not formed at pH 6, no VSFSS measurements were conducted on those samples. In the C-H stretching region, the feature at $\sim 2939 \text{ cm}^{-1}$ is attributed to the methyl symmetric stretch on the backbone of PMAA (Fig. 7A). A small, broad feature at $\sim 2890 \text{ cm}^{-1}$ was necessary when fitting the spectra and is assigned to the methyl symmetric stretch at the end of the polymer tail. Fitted spectra is shown in Fig. S5 (ESI†) with fitting parameters summarized in Tables S4 and S5 (ESI†) that are consistent with previous literature. 34,36,66

As the fitting assignments differ for PAA and PMAA, and therefore individual peak intensities cannot be compared between systems, the integrated intensity in the C-H stretching region was used as a metric for polymer backbone ordering (Table 1). The integrated intensity provides a general representation of polymeric backbone ordering at the emulsion interface. With the same concentration of polymer (500 ppm) at pH 4, adding a methyl group to the polymer backbone results in an increase in the integrated C-H stretching region area. This increase in signal could be attributed to the methyl group on PMAA increasing the solubility of the polymer backbone into the oil phase, therefore improving the polymer ordering. The improved hydrophobic solubility was previously observed by studies of PMAA at the planar oil/water interface.³⁶ However, once increasing the concentration to keep the number of monomer units consistent between PAA and PMAA (2687 ppm), we see a decrease in the integrated area, interpreted as a decrease in the polymer ordering due to the methyl group causing steric hindrance within the polymer backbone. At a lower concentration (500 ppm), PMAA has more space to lengthen and accommodate the additional methyl group, while at a higher concentration (2687 ppm), the methyl group causes a steric disruption to the backbone ordering. At pH 2, we see an overall decrease in the integrated area from PAA to PMAA, regardless of polymer concentration as the addition of a methyl group reduces the interfacial ordering.

Interestingly at pH 6, slight VSFS signal in the C-H stretching region is observed from emulsions coated with 2687 ppm PMAA (Fig. 7A). As this emulsion exhibits short-lived colloidal stability, VSFS spectra measured nearly immediately after formation of the emulsion (20 minutes) was necessary to observe ordered polymer at the interface. The presence of PMAA signal at pH 6 is due to the methyl group on PMAA increasing the oil

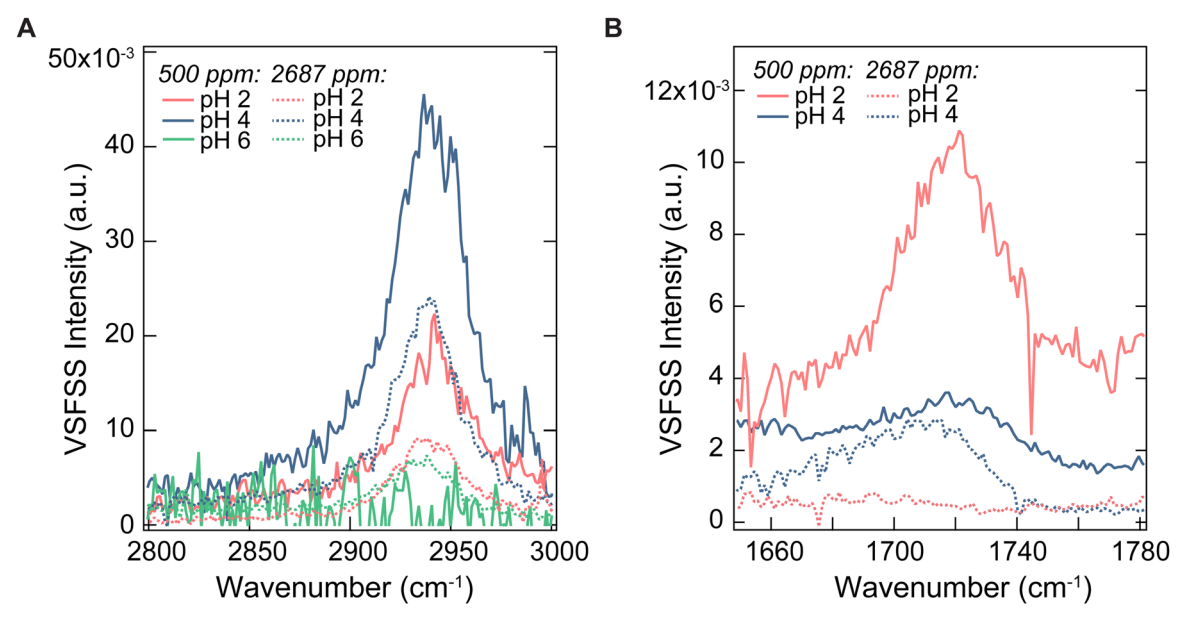


Fig. 7 VSFSS measurements (ssp polarization) of p-hexadecane emulsions in D_2O stabilized with PMAA in the (A) C-H and (B) C=O stretching regions in varying pH conditions. For clarity, spectra are normalized but not fit. Fitted spectra is provided in the ESI.†

Paper

Table 1 Integrated area of VSFSS spectra collected from PAA and PMAA in

the C-H stretching region from 2800-3000 cm⁻¹, corresponding to Fig. 6A

pН	PAA 500 ppm	PMAA 500 ppm	PMAA 2687 ppm
2 4	1.62	1.34	0.559
	1.87	2.84	1.41

solubility at the interface, in contrast to PAA at pH 6 which prefers to be solvated in the water phase due to the deprotonated carboxylic acid groups. While still exhibiting a large negative zeta potential indicative of a deprotonated polymer, the additional methyl group on PMAA aids in oil solvation at the interface leading to a slightly ordered and metastable droplet.

In the C=O stretching region, a single feature at 1736 cm⁻¹ is assigned to the carbonyl stretching mode on the acid (Fig. 7B). With 500 ppm PMAA at both pH 2 and 4, we see a higher intensity for PMAA than was observed for PAA, similar to what was exhibited in the C-H stretching region for pH 4 but opposite to what was observed for pH 2. The C=O intensity suggests that at pH 2, the backbone of PMAA is more disordered due to the steric disruption of the methyl group, but the C=O mode becomes more oriented in the water phase. The lower polymer concentration, as compared to 2687 ppm, allows for accommodation of the increase in steric bulk at the interface and improves the solubility of the methyl group into the oil phase, causing a subsequent ordering of the carboxylic acid group tethered to the backbone at pH 4. Once the monomer concentration is increased (to 2687 ppm), the C=O mode becomes disordered as a result of the polymer backbone steric hindrance causing looping of PMAA. Ultimately, while increasing the hydrophobicity of a polymer improves its solubility at an oil-rich interface at low concentrations, the steric hindrance of the backbone results in enhanced coiling and disorder in

conditions where that behavior is already favorable, such as at high concentration.

Emulsion thermal stability

To be suitable for drug delivery applications, emulsion vessels must withstand variable environments in storage, transport, and infusion into the human body. For example, delivering drugs into the gastrointestinal tract is challenging due to the intense acidity (pH 1-2) of the stomach. 67,68 Additionally, temperature tunability, such as through phase change materials which selectively deposit an agent at a given temperature, is useful for drug delivery systems. 69,70 Here, we show the robust stability of this PAA-coated emulsion system at pH 2 and 4 with varying molecular weights, by measuring the hydrodynamic diameter at a variety of temperatures (Fig. 8). Temperaturedependent PDI is shown in Fig. S5 (ESI†).

Emulsion stability was determined by monitoring the Zaverage diameter as a function of temperature, where an increase in diameter to greater than 1000 nm suggests emulsion coalescence and subsequent instability. This 1000 nm diameter threshold is adapted from the unstable pH 6 emulsions measured in Fig. 1A. Coupled with visual inspection, samples with droplets measuring larger than 1000 nm indicate oil-water phase separation. It should be noted that at pH 2 and 4, all emulsion samples remained well dispersed and turbid over the course of the measurement, indicating colloidal stability regardless of the temperature. Slight increases in diameter were exhibited at lower temperatures (<20 °C) for both pH 2 and 4 in all molecular weights as well as at higher temperatures for 2 and 450 kDa PAA at pH 2. However, these increases are not large enough in magnitude to suggest complete phase separation of the particles and could instead indicate extension of the polymer layer slightly beyond the interface, thus increasing the hydrodynamic diameter but maintaining stable emulsions.

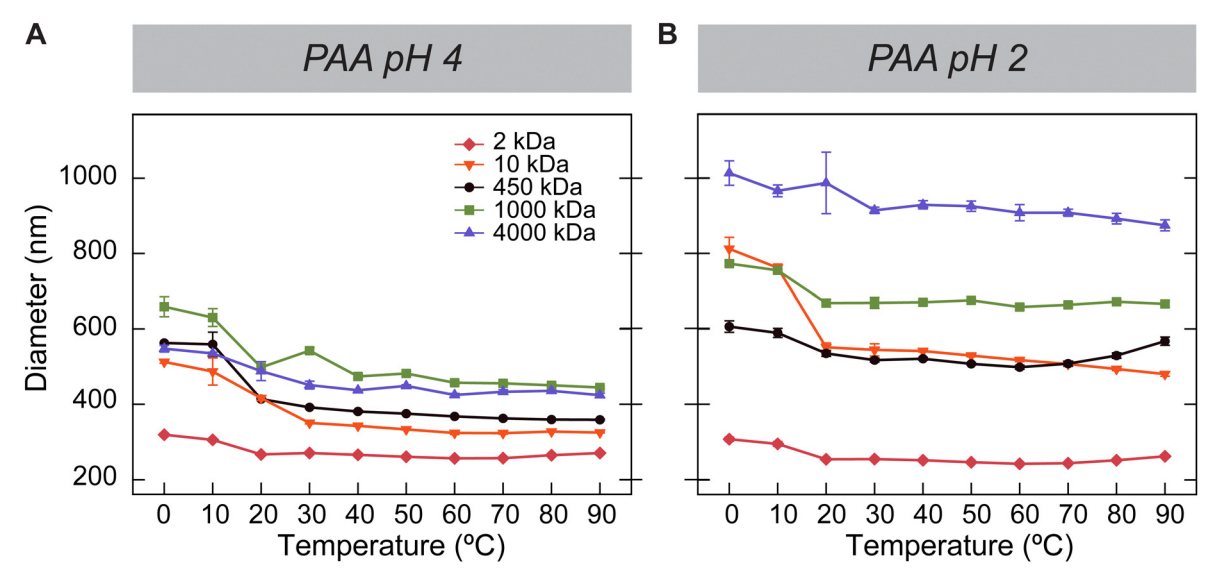


Fig. 8 Diameter of emulsions coated with 500 ppm PAA of varying molecular weight as a function of temperature at (A) pH 4 and (B) pH 2.

Soft Matter Paper

These results are in contrast to other temperature-dependent emulsion studies which observe phase change behaviors at higher temperatures (~60 °C).7 At pH 2, emulsions coated with higher molecular weight PAA exhibit an increasing tendency for layering, resulting in larger droplet sizes. At low molecular weights, where less crosslinking is expected to occur and the polymer behaves more like a surfactant, we see small emulsion sizes. We hypothesize that in addition to forming a steric layer that facilitates colloidal stability at room temperature, the PAA layer provides additional thermal protection, making it a relevant choice for drug delivery. Expanding these results to consider the impact of physiological saline buffers would be useful,71 but we predict from previous work that the addition of electrolyte at low concentrations has minimal impact on the resulting emulsion stability.¹⁰

Conclusion

Via linear and non-linear light scattering techniques, the influence of PAA molecular weight and the addition of a methyl group on the backbone (PMAA) on polymer conformation at the curved hexadecane/water interface was probed. The readily available 450 kDa molecular weight of PAA is considered a standard likely due to its ability to form well-ordered chains at the oil/water interface. At higher molecular weights (1000 and 4000 kDa), enthalpically favored van der Waals interactions between the polymer backbone and the oil as well as hydrogen bonding between polymer chains results in an ordered backbone with multiple polymer layers extending beyond the surface. This surface layering lengthens the hydrodynamic diameter and charge screens the zeta potential. At lower molecular weights (2 and 10 kDa), shorter polymer chains act like surfactants and rely on entropic disorder to solvate the deprotonated groups. This general behavior is exhibited at the natural pH of PAA, pH 4, where no acid or base is added. With PAA at pH 2, the conformational differences as a function of molecular weight are not as distinct due to the nearly 100% protonation of PAA at pH 2 reducing the need for ionic solvation.

For PMAA, with an additional methyl group on the backbone as compared to PAA, no steric hindrance is faced at low concentrations as the polymer has more surface area to extend and form an ordered backbone. In fact, the improved oil solvation of PMAA results in a short-lived emulsion formed at pH 6 with a concentration of 500 ppm PAA. With higher concentration (2687 ppm), making the number of repeat units for PAA and PMAA the same, the additional methyl group causes steric disruption and results in a more disordered configuration as compared to PAA.

The unveiling of polymer conformation at the curved hexadecane/water interface can help design efficient drug delivery emulsions with long-term colloidal stability. In particular, we demonstrate the size stability of these emulsions in physiologically relevant pH and temperature conditions. Another way to tune emulsion stability could be with the incorporation of both short- and long-chain polymers which have been shown to

be impactful for physical properties.⁷² Combining polymers of varying molecular weight could improve interfacial surface coverage due to efficient packing capability, similar to surfactant mixtures and surfactant-polymer composites.

Author contributions

A. N. M.: conceptualization, investigation, methodology, formal analysis, visualization, writing - original draft, and writing review & editing. L. F. S.: conceptualization, funding acquisition, project administration, supervision, and writing - review & editing.

Data availability

All data is provided in the ESI† and available here: Mapile, Ashley (Forthcoming 2024). Bulking Up: The Impact of Polymer Sterics on Emulsion Stability [Dataset]. Dryad. https://data dryad.org/stash/share/iU1bREdZO7v_dsCm7tw38e_17gs55llL 2vvUB iiqnc

Conflicts of interest

There are no conflicts to declare.

Acknowledgements

Thank you to Geraldine Richmond, Konnor Jones, and Priscilla Lewis for insightful conversations. This work is supported by the National Science Foundation under Grant No. CHE 2003526.

References

- 1 A. Fahr and X. Liu, Expert Opin. Drug Delivery, 2007, 4,
- 2 B. Wilson and K. M. Geetha, J. Drug Delivery Sci. Technol., 2022, 74, 103553.
- 3 A. Pourjavadi, S. S. Amin and S. H. Hosseini, *Ind. Eng. Chem.* Res., 2018, 57, 822-832.
- 4 G. Yilmaz, B. Demir, S. Timur and C. R. Becer, Biomacromolecules, 2016, 17, 2901-2911.
- 5 C. Hogarth, K. Arnold, A. McLauchlin, S. P. Rannard, M. Siccardi and T. O. McDonald, J. Mater. Chem. B, 2021, 9, 9874-9884.
- 6 L.-H. Chen and P. S. Doyle, Adv. Mater., 2021, 33, 2008618.
- 7 M. Handa, R. R. Ujjwal, N. Vasdev, S. J. S. Flora and R. Shukla, ACS Omega, 2021, 6, 559-568.
- 8 Q. Huo, Y. Gao, W. Wu, S. Hu, E. Dong, Y. Zhang, Y. Tian, Y. Huang, P. Quan and D. Liu, Adv. Funct. Mater., 2024,
- 9 Y. Miao, L. Li, Y. Wang, J. Wang, Y. Zhou, L. Guo, Y. Zhao, D. Nie, Y. Zhang, X. Zhang and Y. Gan, Nat. Commun., 2024, **15**, 1159.

- 10 A. N. Mapile and L. F. Scatena, *Colloids Surf.*, A, 2024, 697, 134414.
- 11 R. Wang, Q. Wei, W. Sheng, B. Yu, F. Zhou and B. Li, *Angew. Chem.*, *Int. Ed.*, 2023, **62**, e202219312.
- 12 D. Li, L. Xu, J. Wang and J. E. Gautrot, *Adv. Healthcare Mater.*, 2021, **10**, 2000953.
- 13 A. Patel, A. Mohanan and S. Ghosh, *Soft Matter*, 2019, **15**, 9762–9775.
- 14 S. Bochenek, A. A. Rudov, T. Sassmann, I. I. Potemkin and W. Richtering, *Langmuir*, 2023, **39**, 18354–18365.
- 15 H.-G. Seong, Z. Jin, Z. Chen, M. Hu, T. Emrick and T. P. Russell, *J. Am. Chem. Soc.*, 2024, **146**, 13000–13009.
- 16 C. Effenberg and J. Gaitzsch, *Soft Matter*, 2024, **20**, 4127–4135.
- 17 J.-M. Y. Carrillo, Z. Chen, U. I. Premadasa, C. Steinmetz, E. B. Coughlin, B. Doughty, T. P. Russell and B. G. Sumpter, *Nanoscale*, 2023, **15**, 1042–1052.
- 18 T. I. Morozova, N. A. García, J.-L. Barrat, G. S. Luengo and F. Léonforte, ACS Appl. Mater. Interfaces, 2021, 13, 30086–30097.
- 19 H. Qiao, B. Wu, S. Sun and P. Wu, *J. Am. Chem. Soc.*, 2024, **146**, 7533-7542.
- 20 M. Kawaguchi and A. Takahashi, *Macromolecules*, 1983, 16, 1465–1469.
- 21 E. Tran and G. L. Richmond, Langmuir, 2021, 37, 12643-12653.
- 22 J. Xu, L. Bai, W. Ren, H. Zhu, X. Zhou, C. Zhang and X. Wang, *Soft Matter*, 2024, **20**, 201–211.
- 23 M. S. Sulatha and U. Natarajan, *Ind. Eng. Chem. Res.*, 2011, 50, 11785–11796.
- 24 S. Zhu, Z. Ye, Z. Liu, Z. Chen, J. Li and Z. Xiang, *Polymers*, 2021, 13, 1774.
- 25 I. Kirchenbuechler, D. Guu, N. A. Kurniawan, G. H. Koenderink and M. P. Lettinga, *Nat. Commun.*, 2014, 5, 5060.
- 26 M. A. C. Stuart, Polym. J., 1991, 23, 669-682.
- 27 D. Welch, M. P. Lettinga, M. Ripoll, Z. Dogic and G. A. Vliegenthart, *Soft Matter*, 2015, 11, 7507–7514.
- 28 M. J. B. Davis, B. Zuo and R. D. Priestley, *Soft Matter*, 2018, **14**, 7204–7213.
- 29 B. M. de Lima, P. L. Hayes and P. M. Wood-Adams, *Langmuir*, 2021, 37, 10036–10045.
- 30 C. J. Moll, G. Giubertoni, L. van Buren, J. Versluis, G. H. Koenderink and H. J. Bakker, *Macromolecules*, 2021, 54, 8655–8663.
- 31 D. K. Beaman, E. J. Robertson and G. L. Richmond, *Proc. Natl. Acad. Sci. U. S. A.*, 2012, **109**, 3226–3231.
- 32 G. Cavallaro, G. Lazzara and S. Milioto, *Soft Matter*, 2012, **8**, 3627–3633.
- 33 R. Dong, M. Lindau and C. K. Ober, *Langmuir*, 2009, 25, 4774–4779.
- 34 J. Wang, C. Chen, S. M. Buck and Z. Chen, *J. Phys. Chem. B*, 2001, **105**, 12118–12125.
- 35 J. Wang, S. E. Woodcock, S. M. Buck, C. Chen and Z. Chen, *J. Am. Chem. Soc.*, 2001, 123, 9470–9471.
- 36 N. A. Valley, E. J. Robertson and G. L. Richmond, *Langmuir*, 2014, **30**, 14226–14233.

- 37 N. A. Valley and G. L. Richmond, *J. Chem. Theory Comput.*, 2015, **11**, 4780–4790.
- 38 H. J. M. A. Mieras and C. F. H. V. Rijn, *Nature*, 1969, 224, 165–166.
- 39 E. M. Saffer, M. A. Lackey, D. M. Griffin, S. Kishore, G. N. Tew and S. R. Bhatia, *Soft Matter*, 2014, **10**, 1905–1916.
- 40 T. Deplancke, O. Lame, F. Rousset, R. Seguela and G. Vigier, *Macromolecules*, 2015, **48**, 5328–5338.
- 41 T. Kida, Y. Hiejima and K. Nitta, *Macromolecules*, 2021, 54, 225–234.
- 42 A. Krężel and W. Bal, J. Inorg. Biochem., 2004, 98, 161-166.
- 43 S. Roke, W. G. Roeterdink, J. E. G. J. Wijnhoven, A. V. Petukhov, A. W. Kleyn and M. Bonn, *Phys. Rev. Lett.*, 2003, **91**, 258302.
- 44 M. L. Strader, H. B. de Aguiar, A. G. F. de Beer and S. Roke, *Soft Matter*, 2011, 7, 4959–4963.
- 45 Y. R. Shen, Nature, 1989, 337, 519-525.
- 46 A. G. Lambert, P. B. Davies and D. J. Neivandt, *Appl. Spectrosc. Rev.*, 2005, **40**, 103–145.
- 47 A. N. Mapile, M. A. LeRoy, K. Fabrizio, L. F. Scatena and C. K. Brozek, ACS Nano, 2024, 18, 13406–13414.
- 48 E. Tran, A. N. Mapile and G. L. Richmond, *J. Colloid Interface Sci.*, 2021, **599**, 706–716.
- 49 E. J. Robertson and G. L. Richmond, *J. Phys. Chem. C*, 2014, **118**, 28331–28343.
- 50 P. Balzerowski, K. Meister, J. Versluis and H. J. Bakker, *Phys. Chem. Chem. Phys.*, 2016, **18**, 2481–2487.
- 51 NLS-Simulate. Get the software safely and easily., https://nls-simulate.software.informer.com/, (accessed 6 June 2022).
- 52 A. G. F. de Beer, S. Roke and J. I. Dadap, J. Opt. Soc. Am. B, 2011, 28, 1374–1384.
- 53 S. Roke and G. Gonella, *Annu. Rev. Phys. Chem.*, 2012, **63**, 353–378.
- 54 A. N. Mapile, M. A. LeRoy, K. Fabrizio, L. F. Scatena and C. K. Brozek, ACS Nano, 2024, 18, 13406–13414.
- 55 E. Tran, K. K. Jones, G. A. Cano, F. G. Moore and L. F. Scatena, *J. Phys. Chem. B*, 2022, **126**, 7720–7730.
- 56 C. D. Bain, P. B. Davies, T. Hui. Ong, R. N. Ward and M. A. Brown, *Langmuir*, 1991, 7, 1563–1566.
- 57 M. J. Foster, A. P. Carpenter and G. L. Richmond, *J. Phys. Chem. B*, 2021, **125**, 9629–9640.
- 58 C. A. J. Hoeve, E. A. DiMarzio and P. Peyser, *J. Chem. Phys.*, 1965, **42**, 2558–2563.
- 59 V. S. Kravchenko, I. V. Portnov and I. I. Potemkin, *Macromolecules*, 2023, **56**, 7626–7635.
- 60 J. L. Garcés, G. J. M. Koper and M. Borkovec, *J. Phys. Chem.* B, 2006, 110, 10937–10950.
- 61 D. Hu, Z. Yang and K. C. Chou, J. Phys. Chem. C, 2013, 117, 15698–15703.
- 62 A. U. Chowdhury, G. J. Taylor, V. Bocharova, R. L. Sacci, Y. Luo, W. T. McClintic, Y.-Z. Ma, S. A. Sarles, K. Hong, C. P. Collier and B. Doughty, J. Am. Chem. Soc., 2020, 142, 290–299.
- 63 A. Araiza-Calahorra and A. Sarkar, Food Funct., 2019, 10, 5498–5509.

- 65 L. Schmüser, T. W. Golbek and T. Weidner, Biointerphases, 2021, 16, 011201.
- 66 L. Peplowski, R. Szczesny, L. Skowronski, A. Krupka, V. Smokal and B. Derkowska-Zielinska, Vib. Spectrosc., 2022, 120, 103377.
- 67 F. Zhang, Z. Li, Y. Duan, A. Abbas, R. Mundaca-Uribe, L. Yin, H. Luan, W. Gao, R. H. Fang, L. Zhang and J. Wang, Sci. Robot., 2022, 7, eabo4160.
- 68 J. Byrne, H.-W. Huang, J. C. McRae, S. Babaee, A. Soltani, S. L. Becker and G. Traverso, Adv. Drug Delivery Rev., 2021,

- 69 P. K. Bolla, V. A. Rodriguez, R. S. Kalhapure, C. S. Kolli, S. Andrews and J. Renukuntla, J. Drug Delivery Sci. Technol., 2018, 46, 416-435.
- 70 M. Karimi, P. Sahandi Zangabad, A. Ghasemi, M. Amiri, M. Bahrami, H. Malekzad, H. Ghahramanzadeh Asl, Z. Mahdieh, M. Bozorgomid, A. Ghasemi, M. R. Rahmani Taji Boyuk and M. R. Hamblin, ACS Appl. Mater. Interfaces, 2016, 8, 21107-21133.
- 71 M. V. Zyuzin, T. Honold, S. Carregal-Romero, K. Kantner, M. Karg and W. J. Parak, Small, 2016, 12, 1723-1731.
- 72 E. F. D. Sabattié, J. Tasche, M. R. Wilson, M. W. A. Skoda, A. Hughes, T. Lindner and R. L. Thompson, Soft Matter, 2017, 13, 3580-3591.